COVER SHEET

Title: Identifying Scatter Targets in 2D Space using In Situ Phased-Arrays for Guided Wave Structural Health Monitoring

Authors: Eric B. Flynn
Michael D. Todd
Seth S. Kessler
Chris T. Dunn

PAPER DEADLINE: **May 15, 2011**

PAPER LENGTH: 8 PAGES (Maximum)

INQUERIES TO: **Eric B. Flynn**
Metis Design Corporation
10 Canal Park
Cambridge, MA 02141
909-238-0384
ericbflynn@gmail.com

ABSTRACT

Guided Wave Structural Health Monitoring, GWSHM, involves exciting high frequency mechanical waves in plate, beam, or rod-like structures and sensing the scattered response in order to detect, localize, and characterize damage. Through a process of phase-coherent delay-weight-sum similar to that used in some sonar and radar applications, time-domain scattered responses measured at several closely spaced discrete piezoelectric array elements can be transformed into a single two-dimensional signal representation of amplitude (usually strain or voltage) versus distance and look direction. In this two dimensional representation, a single waveform pulse scattered from a single damage target has a predictable approximate shape which is a function of the pulse wavelength and window, and the geometric layout of the sensing array. The full response of an array, including all primary and secondary reflections (or echoes) from damage, can then be approximated by a superposition of shape functions corresponding to a finite set individual scatter targets. In this paper, following a review of the spatial domain transformation process, we describe how one can estimate the amplitude, arrival time, and bearing (arrival direction) of each discrete target through matching pursuit.

INTRODUCTION

One of the most significant challenges in GWSHM is the separation of primary wave scattering due to damage from secondary reflections, or echoes, following

---

Eric B. Flynn, Seth S. Kessler, Chris T. Dunn, Metis Design Corporation, 10 Canal Park, Cambridge MA, 02141, USA

Michael D. Todd, University of California, San Diego, 9500 Gilman Dr, La Jolla, CA, 92093-0085, USA

subsequent interaction with structural features such as boundaries and connection joints [1-3]. Such echoes have the tendency to corrupt GWSHM images by indicating false locations of damage. This study works to address this challenge in three ways: 1) Constructing radial scans, which provide both range and bearing information of potential (true or echoed) scatter sources, through the use of phased transducer arrays, 2) Using matching pursuit to pinpoint discrete scatter targets, and 3) Reducing and eliminating false targets through matched filtering based on the structure geometry.

SENSOR HARDWARE AND INTERROGATION PROCESS

In this study, we specifically consider a structure instrumented with an array of Metis Design MD7 transducer nodes. Each node consists of a single central piezoelectric transducer for actuation encircled by six piezoelectric sensing transducers spaced approximately 7 mm from the center and at 60 degree intervals. One at a time, each MD7 node actuates a series of narrow-band, ultrasonic mechanical pulses using its central actuation transducer. These pulses propagate through the structure, reflect and scatter at geometric features as well as potential damage, and are then sensed by the six sensing transducers on the node. This is repeated for each MD7 node on a structure.

While we specifically consider the use of the MD7 node in the study, the approach we present is relevant for most GWSHM instrumentation involving sets of closely spaced transducer elements. This type of configuration enables one to estimate both the relative range(s) and bearing(s) of potential damage in the structure using only a single tight group of transducers (or node).

TIME DOMAIN PROCESSING

Filter

In order to reduce the influence of both mechanical and electronic noise sources, the waveforms are band-pass-filtered about the actuation frequency. This filtering is performed by passing the signals through a standard digital filter in the forward direction and then again in the reverse direction. This forward and reverse filtering eliminates the signal phase distortion introduced by the filter.

Complex Envelope

Next, the complex envelope is calculated according to:

$$y_{CE}(t) = y_A(t)\exp(-j2\pi f_C t) \tag{1}$$

where $y_A(t)$ is the analytic signal of the filtered waveforms and f_C is the excitation frequency.

Downsample

Since the complex envelope is narrowband, it can be down-sampled to twice the bandwidth of the narrowband excitation pulse without loss of information. The down-sampling substantially reduces the computation and memory requirements for the subsequent processing.

Whiten

Processing of the waveforms is simplified by first transforming the data such that it is approximately zero-mean, complex-normal distributed when damage is not present. This transformation, commonly referred to as whitening, follows the form

$$\boldsymbol{y}_W = \left(\boldsymbol{y}_{CE} - \boldsymbol{\mu}\right)^H \boldsymbol{C}^{-1}, \tag{2}$$

where $\boldsymbol{\mu}$ and $\boldsymbol{C}$ are the mean and covariance (both complex) of the measurement waveforms and usually are estimated using sets of "baseline" waveforms acquired when the structure is in a known-to-be-undamaged state. Note that care must be taken when inverting the estimated covariance matrix, especially when limited baseline waveform samples are available [4].

SPATIAL DOMAIN PROCESSING

Spatial Transformation

The next step is to convert the time-domain measurement waveforms $y_W(t)$ into spatial domain waveforms $w(d)$. In other words, the waveforms will be represented as a function of distance travelled, d, rather than time, t. When using narrowband excitation, and in the presence of minimal dispersion, this can be done by simply scaling the time vector by the wave group velocity at the primary excitation frequency.

In the presence of dispersion, however, the wave velocities are a function of frequency, so the waveforms must be transformed through dispersion compensation. This can be achieved by transforming the time domain signals to the frequency domain through a discrete Fourier transform, using the dispersion curves and interpolation to convert from the frequency domain to the wave-number domain, and taking the inverse discrete Fourier transform to obtain the dispersion-compensated spatial domain signal [5].

Coherent Beamforming

In casex where the distance between sensing transducers satisfies the spatial Nyquist sampling criterion [6], the delayed waveforms can be combined coherently, without enveloping, which is referred to as coherent beamforming [7]. The spatial sampling criterion is usually satisfied with a sensor-to-sensor pitch of less than one half the wavelength of the sensed wave of interest. If we represent the whitened spatial domain waveform from each transducer pair m according to the complex signal $w_{nm}(d)$, then a test statistic for the coherent detector for damage at $\boldsymbol{x}$ reduces to

$$I^{(\mathrm{C})}\left(\boldsymbol{x}\right) = \left| \sum_{m=1}^{M} a_m^{(\mathrm{C})}\left(\boldsymbol{x}\right) w_m\left(d_m\left(\boldsymbol{x}\right)\right) \right| \tag{3}$$

where $d_m(\boldsymbol{x})$ is the total travel distance from transducer pair m to $\boldsymbol{x}$ (from the actuator to $\boldsymbol{x}$ to the sensor) and $a_m(\boldsymbol{x})$ is a weighting function which we assign to be uniformly equal to one for this study. Coherent beamforming is ideal since the summation of the delayed waves tend to destructively combine at all locations except the true location of damage. However, the transducers generally must be very closely

spaced, limiting their coverage of the structure. In practice, for narrowband signals, the time delays are achieved through computationally faster phase shifts.

Incoherent Beamforming

When implementing sparse transducer arrays, the *envelopes* of the waveforms are usually summed together in order to eliminate the dependence on phase. This effectively shifts the signal wavenumber down so that the spatial sampling criterion is met. The test statistic for the incoherent ("phase ignorant") detector for damage at $\boldsymbol{x}$ reduces to

$$I^{(\mathrm{I})}(\boldsymbol{x}) = \sum_{m=1}^{M} a_m^{(\mathrm{I})}(\boldsymbol{x}) \left| w_m\left(d_m(\boldsymbol{x})\right)\right| \tag{4}$$

where again $a_m^{(\mathrm{I})}(\boldsymbol{x}) = 1$ for this study. Sparse arrays are effective at covering large areas of a structure at the cost of reduced imaging resolution.

Hybrid Beamforming

Each MD7 sensor node involves a single actuating transducer surrounded by six sensing transducers. The sensors in each node satisfy the sampling criteria for the excitation frequencies and wave modes of interest, allowing for coherent beamforming. From node to node, however, the criterion is not met and as such the measured signals must be combined incoherently. This hybrid approach enables both effective imaging through coherent beamforming within each node as well as effective coverage of large areas through the placement of multiple nodes. If we represent the sensed and processed waveform from transducer pair m on node n as $w_{nm}(d)$, then the hybrid beamforming test statistic takes the form

$$I^{(\mathrm{H})}(\boldsymbol{x}) = \sum_{n=1}^{N} a_n^{(\mathrm{I})}(\boldsymbol{x}) \left| \sum_{m=1}^{6} a_m^{(\mathrm{C})}(\boldsymbol{x})\, w_{nm}\left(d_{nm}(\boldsymbol{x})\right)\right| \tag{5}$$

Figure 1 shows an example of the imaging of a 8 mm disc diameter magnet on a one meter square plate using incoherent and hybrid imaging with one and three nodes.

In practice, it is more efficient to use local polar coordinates to represent the image generated from a single node. The test statistic image, which now can be thought of as a radial scan, is represented as $I_C(r_n, \theta_n)$, where the radius r_n and bearing θ_n are relative to the centroid of node n. The image can be formed directly from the analytic signals in a manner analogous to (3)

$$I_n^{(\mathrm{C})}(r_n, \theta_n) = \left| \sum_{m=1}^{M} w_{nm}\left(d_{nm}(r_n, \theta_n)\right)\right|. \tag{6}$$

With respect to a given node and for uniformly spaced coordinates, the polar form more accurately reflects the effective resolution of an image than the Cartesian form. This enables more efficient storage and data transfer. More importantly, however, the polar scans provide a natural coordinate domain for further processing, as discussed in the next section. The final processed scans from multiple nodes are then combined on common Cartesian coordinate system through interpolation.

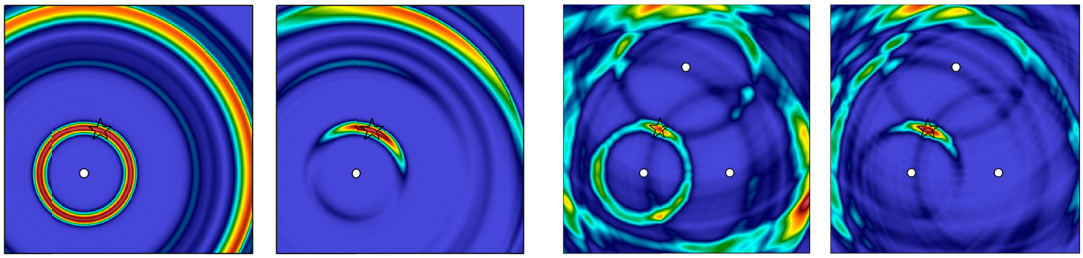

Figure 1: Incoherent and hybrid imaging using one node (A, B) and three nodes (C, D) on a one meter square plate.

Matching Pursuit for Identifying Potential Scatter Targets

The purpose of the matching pursuit algorithm is to decompose the radial scan from each node into a sum of similarly shaped wave reflection packets, so it they may be approximated according to

$$I^*(r,\theta) = \sum_i A_i K(r - R_i, \theta, \vartheta_i) \tag{7}$$

where A_i, R_i, and ϑ_i are estimates of the amplitude, range and bearing of the i^{th} largest scatter "target" and $K(r,\theta,\vartheta_i)$ is the wave reflection shape function. The wave reflection shape function depends on the shape and wavelength(s) of the excitation pulse as well as the layout and weightings of the sensing array elements within each node. The shape function for a Gaussian-windowed sinusoid takes the approximate form

$$K(r,\theta,\vartheta_i) = \exp\left(\frac{-r^2}{2\sigma^2}\right) B(\theta,\vartheta_i) \tag{8}$$

where σ^2 is the width parameter of the excitation and $B(\theta,\vartheta_i)$ is the beamformer response function for steer bearing ϑ_i and measurement bearing θ [6].

Figure 2 shows the shape function for the six-sensor MD7 node with uniform weighting and a wavelength of 30 mm. Note that the beamshape for arrays that are close to radial-symmetric (such as the MD7) is primarily a function of the difference between the steer and measurement bearing, i.e. $B(\theta,\vartheta_i) \approx B(\theta - \vartheta_i, 0)$. One of the significant advantages to working in the polar domain is that is allows one to separate the radial and angular dependence of the shape function.

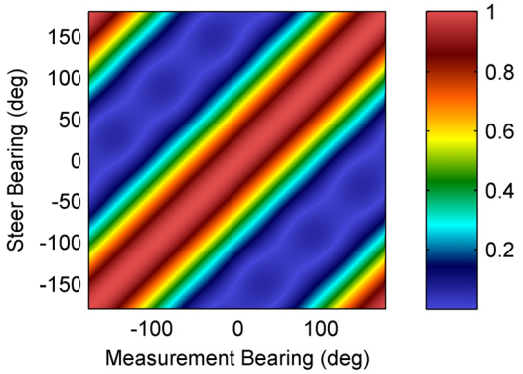

Figure 2: Normalized beamshape for MD7 array and wavelength of 30 mm.

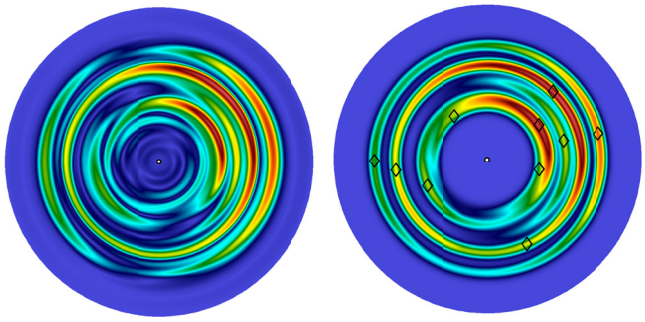

Figure 3: Original MD7 scan (left) and reconstructed scan using ten matching pursuit wave packets (right). Scan radius equal to one meter.

The amplitudes, ranges, and bearings of the wave packets are estimated according to the following matching pursuit algorithm:

1) Identify range, bearing, and amplitude corresponding the global maximum of the radial scan image

$$\{R_i, \vartheta_i\} = \arg\max_{r,\theta} I(r,\theta), \quad A_i = I(R_i, \vartheta_i) \tag{9}$$

2) Subtract the reconstructed wave packet from the radial scan image

$$I(r,\theta) = I(r,\theta) - A_i K(r - R_i, \theta - \vartheta_i) \tag{10}$$

3) Repeat until the error the between the original image and the reconstructed image reaches a minimum

$$P_{Optimal} = \arg\min_{P} \sum_{r,\theta} \left(I(r,\theta) - \sum_{i=1}^{P} A_i K(r - R_i, \theta, \vartheta_i) \right)^2 \tag{11}$$

Figure 3 shows an original radial scan for a single MD7 node and the reconstructed image using ten discrete reflection packets.

Matched Filtering for Eliminating False Targets

As is the case in active sonar and radar, false targets, which are most frequently the result of sensing secondary reflections, or "echoes", from the true target, have the potential to severally corrupt reconstructed images, as is the case in the scan in Figure 3. To reduce the influence of these false targets, we apply a matched filter to the target measurements. Matched filtering consists of multiplying the amplitude of each wave packet by the relative expected amplitude, as measured by each node, if a target was truly present in that location.

PROOF OF CONCEPT

Experimental Setup

The structure used in this study, shown in Figure 4, consists of a 183 cm by 91 cm by 6 mm aluminum plate with two bolted doublers and two large structural through-holes, each of which is encircled by a ring of twelve bolt holes. The plate was

instrumented with four MD7 nodes. Two damage modes were introduced simultaneously by loosening of one of the doubler bolts to finger-tight and the adding a 3 mm notch to one of the encircling bolt holes. This type of structure is can be especially troublesome with respect to secondary echos as waves have a tendency to become "trapped" within the boundaries of the doubler, reflecting back and forth a number of times before being sensed. In the GWSHM images, this leads to what appear to be multiple instances of damage in a line on the opposite side of the doubler from a node.

Procedure and Results

The node actuators were driven with a 60 KHz Gaussian-windowed sinusoid approximately 5.5 cycles in length. The received signals were processed according to procedure outlined above. In the present test, we chose not to presume anything about the potential damage modes and their wave scattering behavior. As such, the matched filter weighting is based primarily on attenuation due to radial beam spreading, interaction with the doubler boundaries, and line of sight. For example, the contribution to identification of a target by a node on the opposite side of the doubler will be significantly scaled down and likely eliminated through thresholding.

Figure 5A shows the raw image generated through hybrid beamforming and Figure 5B shows the reconstructed hybrid image following matching pursuit target identification. As the figure demonstrates, the natural wave reflection shape functions leave a large degree of ambiguity in the target bearing. When the responses from multiple nodes are combined, this leads to significant error in the target localization. To remedy this, the radial scans can alternatively be reconstructed using the same estimated target amplitudes, ranges, and bearings, but with a narrower shape function, as shown in Figure 5C. Here, the precise locations of the potential reflection targets can be more readily identified. Finally, Figure 5D shows the reconstructed image after false target elimination through matched filtering and thresholding of the targets. With the significant reduction in secondary echoes, the two damage modes can now be easily and uniquely identified.

CONCLUSION

The statistical effectiveness of the presented approach has yet to be determined. At worst, it provides a useful qualitative tool for visualizing GWSHM images. At best, it produces a set of nearly-sufficient, very low-order statistics in the form of discrete scatter targets. A more thorough treatment of the problem would involve the determination of statistically optimal beamforming weights and target rejection thresholds. The utility of such an approach is likely highest for the simultaneous detection and localization of multiple damage modes, where common delay and sum approaches suffer from unintentional coherent addition of overlapping damage indicators (as was the case in Figure 5B). Finally, it is possible that the estimated target properties, such as the relative perceived amplitude from different nodes, could aid in the classification of damage when combined with anticipated scattering profiles.

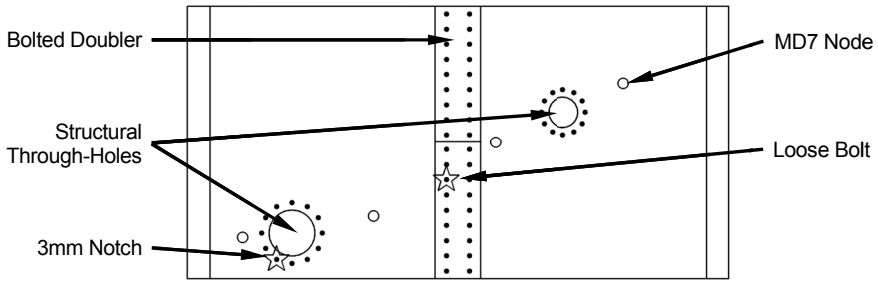

Figure 4: Experimental setup on 183 cm × 91 cm × 6mm aluminum plate with four MD7 nodes

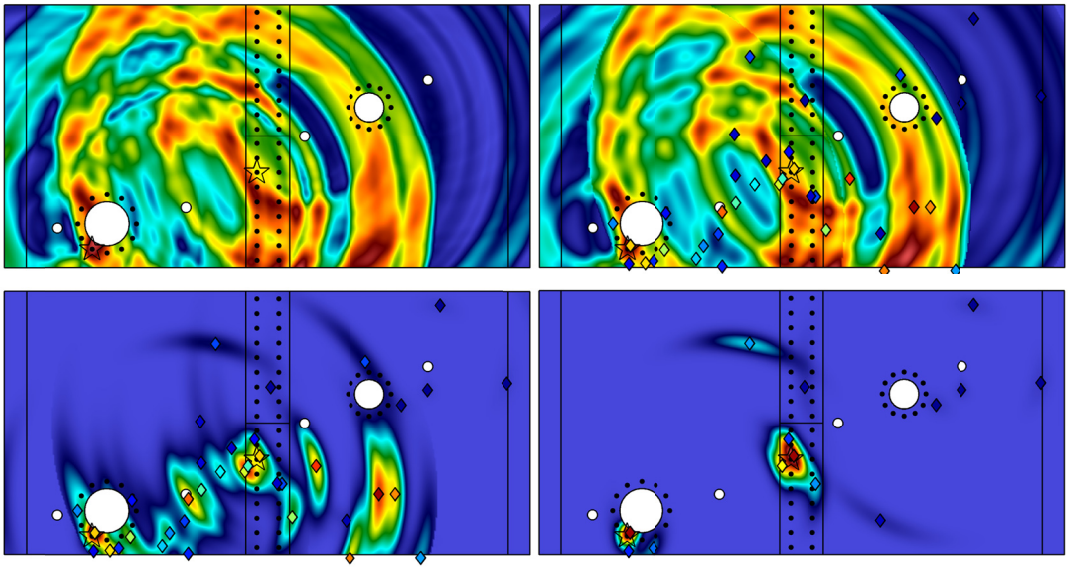

Figure 5 A) Raw ultrasonic image, B) Reconstructed image using matching pursuit-identified targets (diamonds), C) Reconstructed image with reduction in shape function size, D) Reconstructed image with false target rejection through matched filtering.

REFERENCES

1. Flynn EB, Todd MD, Wilcox PD, Drinkwater BW, Croxford AJ. Maximum-likelihood estimation of damage location in guided-wave structural health monitoring. Proceedings of the Royal Society A: Mathematical, Physical and Engineering Science. 2011;
2. Croxford AJ, Wilcox PD, Drinkwater BW, Konstantinidis G. Strategies for guided-wave structural health monitoring. Proceedings of the Royal Society A: Mathematical, Physical and Engineering Science. 2007 Nov 8;463(2087):2961 -2981.
3. Zhao X, Gao H, Zhang G, Ayhan B, Yan F, Kwan C, et al. Active health monitoring of an aircraft wing with embedded piezoelectric sensor/actuator network: I. Defect detection, localization and growth monitoring. Smart Materials and Structures. 2007 Aug;16(4):1208-1217.
4. Twede DR, Hayden AF. Refinement and generalization of the extension method of covariance matrix inversion by regularization for spectral filtering optimization [Internet]. In: Shen SS, Lewis PE, editors. Imaging Spectrometry IX. San Diego, CA, USA: SPIE; 2003. p. 299-306.
5. Wilcox PD. A rapid signal processing technique to remove the effect of dispersion from guided wave signals. IEEE Transactions on Ultrasonics, Ferroelectrics and Frequency Control. 2003;50(4):419–427.
6. Van Trees H. Optimum array processing. New York: Wiley-Interscience; 2002.
7. Holmes C, Drinkwater BW, Wilcox PD. Post-processing of the full matrix of ultrasonic transmit–receive array data for non-destructive evaluation. NDT and E International. 2005;38(8):701–711.